Multiphysics modelling of the Activated Corrosion Products generation and transport in the WCLL PbLi loop with GETTHEM

Fusion Engineering and Design 222 (2026) 115454

Contents lists available at ScienceDirect

Fusion Engineering and Design

journal homepage: www.elsevier.com/locate/fusengdes

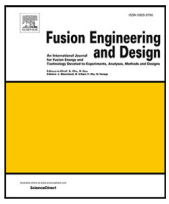

Multiphysics modelling of the Activated Corrosion Products generation and transport in the WCLL PbLi loop with GETTHEM☆

Fabrizio Lisanti [a], Alex Aimetta [a], Pietro Arena [b], Roberto Bonifetto [a], Antonio Froio [a,*]

[a] NEMO group, Dipartimento Energia, Politecnico di Torino, c.so Duca degli Abruzzi 24, 10129, Torino, 10129, Italy
[b] ENEA NUC-ING-PTM, CR Brasimone, Camugnano (BO), 40032, Italy

ARTICLE INFO

Keywords:
EU DEMO
PbLi
Modelling
Activated Corrosion Products
Breeding blanket

ABSTRACT

One of the main milestones towards the development of the EU DEMO reactor is to demonstrate the feasibility of a closed tritium fuel cycle, a key aspect for the generation of electricity from fusion energy by the middle of the century. In view of this, the design of the breeding blanket (BB) has a key role. A candidate design for the EU DEMO BB is the Water-Cooled Lithium-Lead (WCLL) concept, where eutectic lithium-lead (PbLi) is circulated in a suitable closed circuit. A key issue in the design of the PbLi circuit is the evaluation of the inventories of Activated Corrosion Products (ACPs), which are solid particles corroded from structural materials and eventually activated in the blanket, transported inside the loop within the PbLi. In recent years, a PbLi loop model has been implemented in the GETTHEM code, a system-level tool for the thermal-hydraulic modelling of BB and related subsystems. In this work, in addition to the already existing assessment of corrosion phenomena, models of different pieces of physics necessary for a comprehensive assessment of the ACP inventories are added to the PbLi loop model in GETTHEM. Specifically, these include activation and decay of the corroded species in the BB. For the latter, a sink term for the radioactive decay and a source term for the transmutation due to neutrons interaction with materials are introduced in the mass conservation equations for each ACP. To demonstrate the code capabilities, a representative test case is presented.

1. Introduction

One of the concepts that have been proposed for the EU DEMO Breeding Blanket (BB) is the Water-Cooled Lithium-Lead (WCLL) BB [1]. A key aspect for a Lithium Lead (PbLi) based BB is related to the corrosion due to the presence of a flowing liquid metal. When combined with the highly energetic neutrons from the plasma chamber, the corrosion process leads to the generation of Activated Corrosion Products (ACPs) within PbLi. In fact, many activation reactions are threshold reactions (see Fig. 1), meaning that they occur only when highly energetic neutrons interact with the surrounding matter. Thus, the presence of a fast neutron flux can make the issue of ACPs a more serious problem in fusion reactors than in fission reactors. Ultimately, the importance of modelling lies in the fact that ACPs are an important source of radiological hazard and so they are fundamental inputs to safety assessment of nuclear systems. Moreover, the compresence of different physics in the WCLL BB (e.g., thermal-hydraulics, magneto-hydro-dynamics and neutronics) reflects in the need of system-level tools capable of modelling all the different phenomena occurring in the BB, like the generation, transport and removal of ACPs in the WCLL BB PbLi loop.

The General Tokamak Thermal-hydraulic Model (GETTHEM) [2] is under development at Politecnico di Torino since 2015, aiming at the thermal-hydraulic modelling of the BB (and related sub-systems) at a system level. The code has been adopted in the past to study relevant thermal-hydraulic transients of the HCPB and WCLL BB cooling systems [2,3]; also, a model of the WCLL lithium-lead (PbLi) loop, inclusive of MHD pressure drop, was introduced [4]. Recently, the PbLi loop model has been extended to include models for the transport and extraction of tritium from PbLi [5], and for the assessment of the generation and transport of ACPs within the liquid metal, to provide a more comprehensive representation of the PbLi loop. The ACP generation and transport model described in [6] included the mass conservation equation for the corrosion products, where a source term due to corrosion of solid particles from structural materials is implemented by means of the Sannier correlation [7]. In the second test case presented in [6], the overconservative assumption that all the corroded species are activated was made.

☆ This article is part of a Special issue entitled: 'SOFT 2024' published in Fusion Engineering and Design.

* Corresponding author.
E-mail address: antonio.froio@polito.it (A. Froio).

https://doi.org/10.1016/j.fusengdes.2025.115454
Received 17 January 2025; Received in revised form 30 July 2025; Accepted 17 September 2025
Available online 30 September 2025

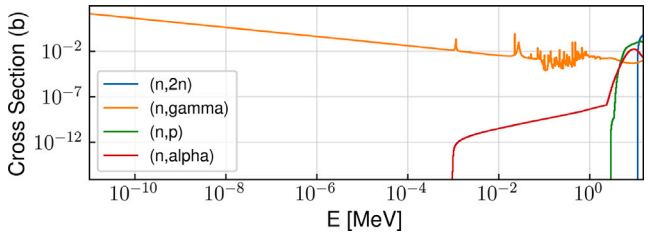

Fig. 1. Cross sections of the main activation reactions of ^{56}Fe.

In this work, the ACP generation and transport model is expanded to include two additional source terms in the ACP mass conservation, accounting for: (i) the activation, in the BB, of the corroded species flowing within the PbLi due to the neutron flux coming from the plasma, and (ii) the decay of the radioactive corrosion products. Thanks to this new model, it is possible to determine the quantity, the activity and the location of the ACPs in the PbLi loop during both normal and off-normal scenarios. To the best of the authors' knowledge, this is the first example of a system-level model for the generation and transport of ACPs in the WCLL PbLi loop.

The implementation of the ACP GETTHEM model aims to fill a gap in literature by providing a comprehensive, dynamic, system-level tool capable of assessing the dynamic evolution of ACPs in the WCLL PbLi loops. Compared to simplified 0D or static approaches, the present work allows simulating multiple physical processes – including thermal-hydraulics, corrosion, neutron-induced activation, and radioactive decay – within a single consistent tool. By discretizing the PbLi loop into 1D control volumes, the model allows spatially resolved estimates of corrosion rates and activation sources based on local flow conditions and neutron spectra in the BB. The model is flexible enough to support further segmentation of BB objects into different poloidal zones, allowing for more refined assessments based on zone-specific neutron fluxes if available. Moreover, the closed-loop configuration enables a self-consistent modelling of ACP recirculation, removal in the cold trap, and transient buildup of corrosion products across all components. These capabilities offer a significant advantage over other estimation methods that typically rely on fixed boundary conditions or globally averaged fluxes. In future work, comparisons with simplified analytical models will be performed to further validate and benchmark the model.

2. Description of the ACP model

The Modelica modelling language has been selected to write the GETTHEM code, being it particularly suitable for the modelling of complex systems thanks to its modular, object-oriented nature, that enables to build new models by simply extending and manipulating existing objects. As a consequence, also the model for the generation and transport of ACPs implemented in GETTHEM has been developed in the Modelica language, relying on the free and open source Modelica Standard Library [8]. In this way, it has been possible to build the new objects required to model ACPs extending already existing 1D and 0D models for typical components of hydraulic circuits.

A 1D flow model of a pipe including the generation and transport of ACPs has been developed adding, to the traditional mass, momentum and energy conservation equations for the liquid metal flow, also the 1D mass conservation for the ACPs transported by the PbLi flow, adopting the Finite Volume (FV) method [6]. The conservation equation for the generic jth dispersed material (DM) in the ith control volume (CV) is written as:

$$\frac{dM_{DM_j,i}}{dt} = \dot{m}_{DM_j,i,in}(t) - \dot{m}_{DM_j,i,out}(t) + S_{C_j,i}(t) + S_{A_j,i}(t) + S_{D_j,i}(t) \quad \forall j \in [1, N_s], \forall i \in [1, N_V] \tag{1}$$

where $M_{DM_j,i}$ is the mass of the jth corroded species in the ith CV, $\dot{m}_{DM_j,i,in/out}$ the mass flow rate of the jth species entering and exiting the ith CV and $S_{C_j,i}$ (in kg/s) the local corrosion source for the jth DM species, obtained from the corrosion rate (in m/s) computed e.g. by means of the Sannier correlation [7]. Sannier's equation field of applicability is limited to cases where the PbLi flows at velocities up to 0.3 m/s and in a temperature range between 370 °C and 550 °C, but the model is flexible allowing the use of different, more suitable correlations, if available. The two terms accounting for the activation of the corroded particles dispersed in the PbLi, when exposed to the neutron flux in the BB, and for their radioactive decay, are $S_{A_j,i}$ and $S_{D_j,i}$: the activation and the decay of the jth species in the ith CV, respectively. The two terms $S_{A_j,i}$ and $S_{D_j,i}$, expressed in kg/s, are defined as:

$$S_{A_j,i}(t) = \sum_{\substack{k=1 \\ k\neq j}}^{N_S} \sigma_{i,j\leftarrow k} \cdot \Phi_i(t) \cdot M_{DM_i,k}(t) - \sigma_{i,j} \cdot \Phi_i(t) \cdot M_{DM_i,j}(t) \quad \forall j \in [1, N_s], \forall i \in [1, N_V], \tag{2}$$

$$S_{D_j,i}(t) = \sum_{\substack{k=1 \\ k\neq j}}^{N_S} \lambda_{j\leftarrow k} \cdot M_{DM_i,k}(t) - \lambda_j \cdot M_{DM_i,j}(t) \quad \forall j \in [1, N_s], \forall i \in [1, N_V], \tag{3}$$

where $\Phi_i(t)$ represents the total neutron flux (in neutrons/m^2/s) in the ith CV, $\sigma_{i,j\leftarrow k}$ (in m^2) denotes the nuclear cross section for the activation reaction undergone by the kth DM producing the jth DM in the ith CV, $\sigma_{i,j}$ the total transmutation cross section of species j (obtained summing the cross sections of all the reactions leading to the transmutation of species j) in CV i, $\lambda_{j\leftarrow k}$ is the decay constant of the kth DM producing the jth DM and λ_j the decay constant of species j. The cross sections σ are functions of space too, since they depend on the neutron flux, as will be explained in the following, differently from the decay constants λ which are space-independent.

The total neutron flux $\Phi_i(t)$ is obtained simply by integrating over the energy domain the neutron spectrum $\phi_i(E,t)$ of the system under study, previously evaluated with a generic neutronic code (in this case, the Monte Carlo code MCNP [9] has been used). Cross section $\sigma_{i,j\leftarrow k}$ (and, in an analogous way, $\sigma_{i,j}$ too) is calculated collapsing the continuous energy cross sections $\sigma_{j\leftarrow k}(E)$ contained in nuclear data libraries (e.g., JEFF-3.3 [10] and ENDF-B/VIII.0 [11]), over the whole energy domain, exploiting the neutron spectrum of the system, as:

$$\sigma_{i,j\leftarrow k} = \frac{\int_0^\infty \sigma_{j\leftarrow k}(E)\phi_i(E)dE}{\int_0^\infty \phi_i(E)dE}, \tag{4}$$

This approach preserves the neutron reaction rates, hence the physics, of the system, even though the continuous energy cross sections are collapsed into discretized mono-energetic values. The procedure of collapsing the continuous energy cross section can be done straightforwardly with the NJOY nuclear data processing code [12,13]. It is important to notice that the continuous energy cross sections $\sigma_{j\leftarrow k}(E)$ depend only on the neutron incoming energy, while the collapsed ones $\sigma_{i,j\leftarrow k}$ are also a function of space, since they are related to the neutron spectrum which changes from component to component.

Concerning the 0D model of the Cold Trap (CT) for the ACP removal from the PbLi flow developed in [6], note that it does not distinguish between the different isotopes of a given chemical element: it will remove, as in reality, the chemical element as a whole. Therefore, it has not been modified. It computes the concentration of the jth species as a function of the inlet concentration, assuming a constant removal efficiency η when the inlet concentration of the jth species is larger than its saturation concentration C_j^s in PbLi:

$$C_{j,out} = \begin{cases} C_{j,in} & \text{for } C_{j,in} < C_j^s \\ C_j^s + (1-\eta_j)(C_{j,in} - C_j^s) & \text{for } C_{j,in} > C_j^s, \end{cases} \tag{5}$$

where $C_{j,in/out}$ are the inlet and outlet concentrations of the jth species, defined as the ratio between the mass of the jth species and the mass of PbLi.

3. Test case

The ACP generation (with special reference to decay and activation) and transport equations implemented in GETTHEM have been tested in a model of the PbLi circuits of the outboard (OB) and inboard (IB) regions of the WCLL concept for the EU DEMO BB [14,15]. Only the detailed models of the components strictly necessary for the analysis of the ACP generation, transport and removal are included.

3.1. Test case description

The current WCLL concept configuration foresees 16 BB sectors, each one comprising three segments in the OB region (left – LOB –, central – COB – and right – ROB) and two in the IB region (left – LIB – and right – RIB). The sectors are fed by four PbLi loops for the OB segments (each loop feeding 12 segments) and two PbLi loops for the IB segments (each loop feeding 16 segments). The PbLi, coming from the main equipment region, is pumped to the lower ring manifold before entering the segments through the inlet legs. Inside the segments, the PbLi is distributed to the breeding zone, divided into breeding units (BUs) by toroidal-radial stiffening plates, where the fluid follows a radial, U-shaped path around baffle plates in the BUs. The PbLi then exits the segments through outlet legs and returns to the main equipment region via the upper ring manifold.

The IB and OB loop models employed in this work are shown in figure Figs. 2(a) and 2(b) respectively. The two models are composed by the components of the main equipment region (i.e., two heat exchangers, the Tritium Extraction and Removal – TER – system, the system for the removal of ACPs, circulation tank and pump), the distribution pipes (i.e., ring manifolds, inlet/outlet legs) and the BB segments. Instead, the PbLi storage tanks is excluded by the model since the test case simulates only the normal operation of the system.

The TER system object does not include the model of the tritium extractor (which is, however, already implemented in GETTHEM [6]), but consists of a simple 1D pipe model. This simplification was adopted because the focus of this work is on the generation and transport of ACPs, rather than tritium-related aspects. In this way, the number of equations to be solved in the model is significantly reduced. The two heat exchangers (HX1 and HX2) have been modelled as ideal ones, i.e. with a constant secondary side temperature of 330 °C, while the 0D model of the cold trap for the removal of activated species is that described in [6].

To reduce the computational cost of each simulation, it is assumed that the dimensions of the BUs are uniform within each segment and equal to those on the equatorial plane. The BB segment models (see BB_COB, BB_LOB, BB_IB in Fig. 2(a)) are composed of the series connection of a model for the BUs, one for the inlet manifold and one for the outlet manifold, each of these consisting of the 1D pipe object described by the new activation model discussed in Section 2. The LIB and RIB segments composing the IB region are identical and, thus, modelled with one object (Fig. 2(a)); the COB and L/ROB segments are modelled by two objects (with LOB and ROB being identical). Within the OB loop model, the L/ROB and COB BB objects are hydraulically in parallel. In this work, corrosion is modelled in all the pipes of the loop where PbLi flows, while activation is assumed to occur only in the objects modelling the BB segments, where the neutron flux is the highest.

This test case is mainly devoted to present the capability of the model to assess the generation and transport of ACPs, not to provide final results in the WCLL PbLi loops. For this reason, only a limited, yet representative, set of activation reactions (listed in Table 1) have been modelled: the main reactions involving ^{56}Fe and ^{54}Fe, as iron is

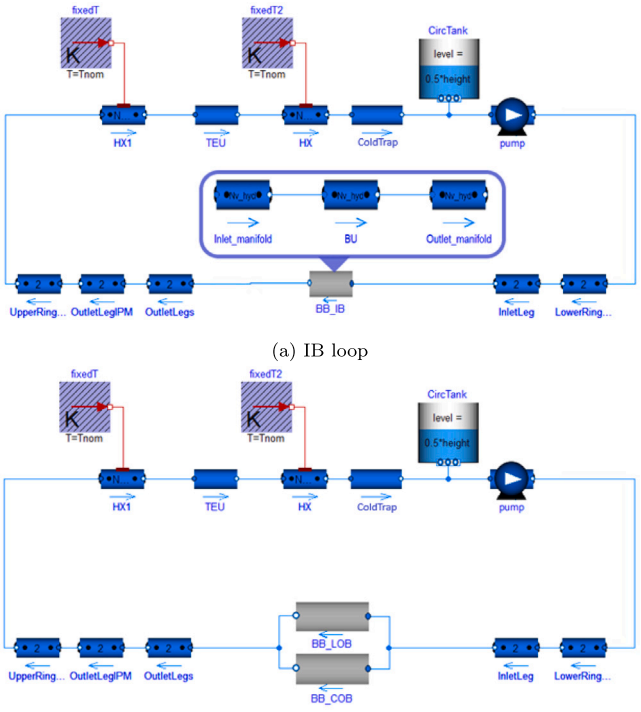

Fig. 2. Scheme of the models of the EU DEMO WCLL PbLi loops: (a) IB loop model with detailed view of the BB object, and (b) OB loop model.

the most abundant element in structural materials, as well as those involving manganese and tungsten, since ^{56}Mn and ^{187}W are significant contributors to the total radiological dose in the WCLL PbLi loops [16]. Moreover, the Sannier correlation has been adopted to estimate corrosion rates, despite some operating conditions in the loop falling outside its applicability range (e.g., PbLi temperature of 330 °C, below the lower bound of 370 °C, and velocities in some regions above 0.3 m/s). This choice is justified by the lack of alternative empirical correlations for PbLi under WCLL-relevant conditions, and by the solely demonstrative nature of the present study. However, the model is flexible enough to easily allow the use of alternative, more suitable correlations – if and when they become available – in future works.

The PbLi is assumed to uniformly corrode the EUROFER97 surfaces of the breeding blanket and the stainless steel surfaces (ASTM A335 P22 was considered in this work) of the loop pipes, hence the corrosion mass source term for each corroded isotope X_k of a given element X is obtained by scaling the total corrosion mass source term S_C (obtained here from Sannier correlation [7]) according to the nominal concentration of the element in the structural material $C_{X,s.m.}$ (e.g. 89% in EUROFER97 and 96 % in ASTM A335 P22 for iron) and the isotopic abundance (f_{X_k}), as:

$$S_{C,X_k} = C_{X,s.m.} \cdot f_{X_k} \cdot S_C \tag{6}$$

All elements and isotopes included in the corrosion source term in this work are listed in Table 2, along with their concentration in structural materials and isotopic abundance. The most abundant isotopes of Fe and Cr are considered, being the primary constituents of structural materials, as well as ^{55}Mn and ^{186}W, due to their role in the activation reactions producing the short-lived radionuclides ^{56}Mn and ^{187}W. Note that ^{50}Cr and ^{52}Cr, despite being stable and not involved in the activation reactions considered in this work (see Table 1), are still included in the model to have a better estimate of the total inventory of Cr inside the circuit, needed to compute its removal from PbLi in the CT

Table 1
Nuclear inputs (average values in BZ and manifolds) used for activation and decay calculations for the test case. EC: electron capture decay mode, β^-: beta-minus decay mode, β^+: beta-plus decay mode. 1 b = 10^{-24} m^2. Note that ^{51}V and ^{187}Re are not considered in this work as transported species within PbLi, since they are stable isotopes and, hence, not radiologically relevant.

Isotope	Reaction	Product	$\bar{\sigma}$ (b) - OB BZ	$\bar{\sigma}$ (b) - OB manifolds
^{54}Fe	(n,n'p)	^{53}Mn (3.74e6 y, EC/β^+) → ^{53}Cr	1.56E−01	1.42E−02
	(n,p)	^{54}Mn (312.3 d, EC/β^+) → ^{54}Cr	1.32E−01	1.99E−02
	(n, α)	^{51}Cr (27.7025 d, EC/β^+) → ^{51}V	2.11E−03	3.74E−04
^{56}Fe	(n,2n)	^{55}Fe (2.73 y, EC/β^+) → ^{55}Mn	1.23E−01	1.09E−02
	(n,n'p)	^{55}Mn	1.83E−02	1.56E−03
	(n,p)	^{56}Mn (2.5785 h, β^-) → ^{56}Fe	3.14E−02	3.38E−03
	(n,d)	^{55}Mn	1.84E−03	1.66E−04
	(n, α)	^{53}Cr	1.29E−03	2.00E−04
^{55}Mn	(n,2p)	^{54}Mn (312.3 d, EC/β^+) → ^{53}Cr	1.88E−01	1.76E−02
	(n,n'p)	^{54}Cr	1.16E−02	1.04E−03
	(n, γ)	^{56}Mn (2.5785 h, β^-) → ^{56}Fe	3.36E−03	6.88E−03
^{56}Mn	(n,2n)	^{55}Mn	3.00E−01	3.13E−02
^{186}W	(n, γ)	^{187}W (23.719 h, β^-) → ^{187}Re	3.12E−02	5.61E−02

Table 2
Isotopic abundances of corroded species and their concentration in structural materials.

	^{54}Fe	^{56}Fe	^{50}Cr	^{52}Cr	^{53}Cr	^{54}Cr	^{55}Mn	^{186}W
Isotopic abundance f_{X_k} [%]	5.8	91.72	4.4	83.8	9.5	2.4	100	28.4
Concentration C_X in EUROFER97 [%]	89			8.93			0.44	1.15
Concentration C_X in ASTM A335 P22 [%]	96			1.77			0.6	0

model. Concerning tungsten, instead, an expression for its saturation concentration in PbLi is not available in literature – to the best of the author's knowledge – so it is currently assumed that CT does not remove W particles. Consequently, other stable tungsten isotopes are not modelled in this work.

The saturation concentrations C_j^S of Fe, Cr and Mn required by the CT model for the removal of ACPs (Eq. (5)) are computed according to [17]:

$$C_{Fe}^S = 10^{-6}\exp\left(13.604 - \frac{12975}{T}\right) \tag{7}$$

$$C_{Cr}^S = 4.92 \cdot 10^{-8}\exp(0.0058T) \tag{8}$$

$$C_{Mn}^S = 10^{-6} \cdot 10^{\left(6.732 - \frac{2938}{T}\right)} \tag{9}$$

where T is the local temperature of PbLi expressed in K and the saturation concentrations C_j^S are expressed in $\mathrm{kg}_{DM}/\mathrm{kg}_{PbLi}$.

The neutron spectra needed for the assessment of the activation source term have been computed by ENEA in different positions of the Breeding Zone (BZ) and inlet/outlet manifolds [18], using the MCNP DEMO WCLL model [19] and employing the VITAMIN-J 175 energy groups grid, specifically developed for fusion blanket shielding [20]. All spectra were evaluated at the equatorial plane, assuming negligible variations of neutron flux in the poloidal direction compared to the radial one. These data have been provided for three locations within the BZ (near the First Wall (FW), in the middle and close to the manifolds) and two locations within the manifolds. As an example, the spectra evaluated with MCNP in the IB and provided by ENEA are shown in Fig. 3, where it is clear that the decrease of the flux at high energies corresponds to the transition from regions nearer to the plasma (FW) to farther ones (manifolds). The results provided by ENEA have a statistical error smaller than 5%, except for low energies where, however, the neutron flux is almost negligible.

For the GETTHEM simulations, the spectra are assumed constant during the simulated transient. Average values of the neutron flux ($\bar{\Phi}$) and cross sections ($\bar{\sigma}_j$) in the BZ and in the manifolds have been adopted:

$$\bar{\Phi} = \frac{\sum_{i=1}^{N_V} \Phi_i \cdot V_i}{\sum_{i=1}^{N_V} V_i} \tag{10}$$

$$\bar{\sigma}_j = \frac{\sum_{i=1}^{N_V} \sigma_{i,j} \cdot \Phi_i \cdot V_i}{\sum_{i=1}^{N_V} \Phi_i \cdot V_i}, \tag{11}$$

where N_V is the total number of volumes over which the average is computed, V_i is the ith volume, Φ_i the total neutron flux (i.e., integrated over the whole energy domain) in the volume V_i, and $\sigma_{i,j}$ the cross section of the jth reaction in volume V_i. As an example, the nuclear inputs in the OB BZ and manifolds used in the GETTHEM WCLL PbLi loop models are reported in Table 1.

3.2. Results

Assuming an initial concentration of dispersed materials in the working fluid equal to zero and a constant rotational speed of the pump, the models of the IB and OB PbLi loops developed for this test case have been used to simulate a transient of 30 days, with a computational time in the order of 10 min. The operating temperature adopted for the simulations is 330 °C, as it is the reference value currently assumed in the design of the WCLL PbLi loops (as reported, e.g., in [21]). The geometrical data and all the other inputs required to run the WCLL PbLi loop models are reported in Table 3.

Fig. 4 shows the concentration evolution of the iron isotopes at the inlet and outlet of the CT for the removal of ACPs, for both IB and OB loops. After ∼ 5 h of transient, the concentrations of all the dispersed iron isotopes have already reached the steady-state in both the loops, since they exceeded the saturation concentration C_{Fe}^S (equal to $3.7 \cdot 10^{-4}$ wppm at the operative temperature of the PbLi loop of 330 °C), allowing the system for the removal of ACPs to extract iron particles from the PbLi flow.

According to the Sannier correlation, higher fluid velocities lead to higher corrosion rates. In the ex-vessel loop piping, PbLi flows at velocities up to 0.54 m/s in the OB loop and 0.48 m/s in the IB, while inside the BB the flow is significantly slower, around 0.3 mm/s in the BZ. Since the IB loop includes longer ex-vessel piping, the overall corrosion rate is larger, resulting in a faster buildup of ACPs. As a result, iron reaches steady-state concentration in the IB loop about two hours earlier than in the OB loop. Additionally, a distinct "staircase" pattern is observed in Fig. 4, caused by the different corrosion rates and PbLi transit times within the series of components undergoing corrosion. In particular, the time intervals where the concentration profile remains

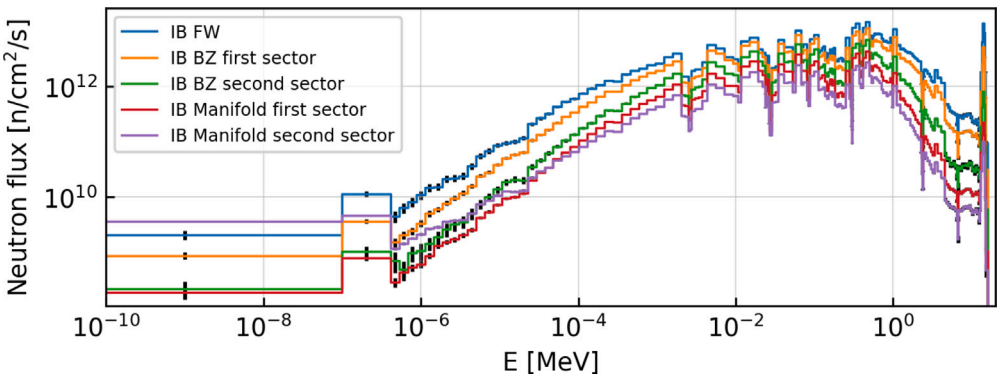

Fig. 3. Neutron spectra (provided by ENEA [18]) in the IB, evaluated on the VITAMIN-J energy grid. The error bars represent the 2σ statistical error.

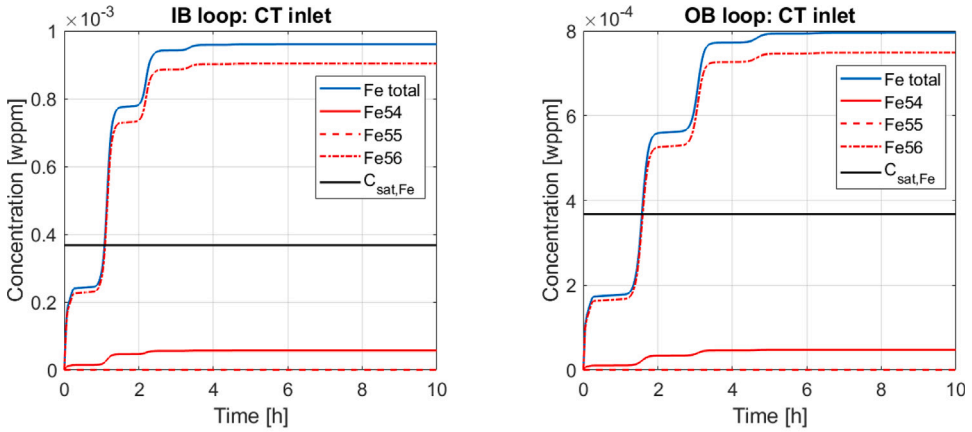

Fig. 4. Evolution of iron concentration at the inlet of the system for the removal of ACPs (modelled here by the CT object, see Section 2), for (a) IB circuit and (b) OB circuit; iron saturation concentration is shown with a black line.

relatively constant correspond to PbLi passing through BUs: here, the corroded mass of iron is limited by the short path of the fluid and by the low flow velocity of $\sim 0.3\,\mathrm{mm/s}$ (which also entails a long transit time of PbLi inside the component).

As shown in Fig. 5(a) almost all the Mn circulating in the loop is ^{55}Mn, suggesting that the corrosion source term is much greater than the activation source term producing the other Mn isotopes. However, even small traces of those radionuclides, particularly ^{56}Mn, can have a substantial impact on the overall radioactivity in the PbLi loop. A similar observation applies to the evolution of tungsten concentration shown in Fig. 6, where ^{186}W accounts for nearly all the tungsten present in PbLi. Nevertheless, the short half-life of ^{187}W still makes its presence radiologically significant for this study. By the end of the simulated time frame (i.e. 30 days), during which a constant neutron flux in the BB is conservatively assumed, the concentration of Mn had only reached approximately $2 \cdot 10^{-3}$ wppm, well below its saturation limit in PbLi (72.60 wppm at 330 °C). In Fig. 5(b) it is interesting to observe the behaviour of ^{56}Mn. The (average) rate of increase of the concentration of this radioactive isotope reduces significantly after ~ 1 day of transient, differently from that of the other Mn isotopes that continue increasing at an almost constant rate. This is mainly due to the much shorter half-life of ^{56}Mn, in the order of few hours (see Table 1), and to the fact that the main source of ^{56}Mn is the activation of ^{56}Fe, whose concentration reaches a steady state value after 5 h. A similar behaviour is expected for other isotopes as well, although after much longer transients.

In analogy with manganese, the chromium concentration at the end of the transient is much smaller than the saturation one (0.01 wppm versus 1.63 wppm at 330 °C). Fig. 7 shows the buildup of the radioactive ^{51}Cr.

Finally, exploiting the capability of the model to compute ACP concentrations during the simulated transient in various locations within the PbLi loops, an assessment of the activity of the species transported within the PbLi flow in the different BB segments and loop pipes has been performed in this test case. The specific activity in $\mathrm{Bq/m^3_{PbLi}}$ of a nuclide X has been computed as:

$$A_X = \lambda_X \cdot N_X = \lambda_X \cdot \frac{C_X \cdot \rho_{PbLi} \cdot N_{AV}}{m_{A,X}}, \tag{12}$$

where λ_X is the decay constant of active nuclide X, N_X the atomic density of nuclide X per unit volume of PbLi, C_X the concentration of isotope X in units of $\mathrm{kg_X/kg_{PbLi}}$, ρ_{PbLi} the mass density of PbLi, N_{AV} the Avogadro constant and $m_{A,X}$ the atomic weight of X. Fig. 8 shows the concentration and the specific activity of the isotopes considered in this work, computed at the cold trap inlet of the OB loop after 30 days of transient. For the sake of brevity, only the results at the inlet of the cold trap, where the activities are the highest, since activated products are partly removed in the cold trap, are shown here. It is interesting to observe that a lower concentration sometimes corresponds to higher values of specific activity, like in the case of ^{56}Mn, ^{51}Cr and ^{187}W. The extremely high activity of ^{56}Mn is also consistent with its concentration evolution in Fig. 5. This result suggests that, in the future, also the activation of chromium should be taken into account to have a more representative picture of the ACPs in the EU DEMO WCLL BB.

The trends observed in the evolution of iron, manganese, chromium and tungsten concentrations in the PbLi loop, shown in Figs. 4–7, and the specific activities (Fig. 8), are qualitatively consistent with

Table 3
Input parameters for test case.

	IB LOOP	OB LOOP	
BB			
Number of segments per loop	16	8 (LOB+ROB), 4 (COB)	–
Number of BUs per segment	92	104 (COB), 103 (L/ROB)	–
BU channel length	0.358	0.548 (COB), 0.539 (L/ROB)	m
BU channel hydraulic diameter	0.088	0.098 (COB)	m
Inlet/Outlet manifold length	12.565	14.154 (COB), 13.989 (L/ROB)	m
Average neutron flux	3.51E+18 (BU), 9.71E+17 (manifolds)	2.52E+18 (BU), 3.13E+17 (manifolds)	$n/(m^2s)$
COLD TRAP			
Pipe length	0.4	0.4	m
Pipe diameter	0.250	0.250	m
ACP removal efficiency	0.9	0.9	–
PUMP			
Nominal rotational speed	1200	1200	r.p.m
Nominal fluid density	9802.6	9802.6	kg/m^3
Nominal head	1.2	1.2	bar
Flow characteristic: H: head [m], Q: vol. flow rate [m^3/s]	$H = -262.3\,Q^2$ $-2.2616\,Q$ $+1.3215$	$H = -335.0\,Q^2$ $-2.5556\,Q$ $+1.3215$	
HEAT EXCHANGERS			
Secondary side temperature	603.15	603.15	K
Pipe length	0.5	0.5	m
Pipe diameter	0.250	0.250	m
TER			
Pipe length	40	40	m
Pipe diameter	0.3	0.3	m
CIRCULATION TANK			
Height	10	10	m
Initial level	5	5	m
Surface pressure	4.2	4.2	bar
Cross sectional area	1	1	m^2
PbLi FLOW			
Nominal mass flow rate	249.3	281.7	kg/s
Nominal pressure	46	46	bar
Nominal temperature	603.15	603.15	K
LOWER RING MANIFOLD			
Pipe length	65	50	m
Pipe internal diameter	258.8	258.8	mm
Number of pipes per loop	1	1	–
UPPER RING MANIFOLD			
Pipe length	65	50	m
Pipe internal diameter	258.8	258.8	mm
Number of pipes per loop	1	1	–
INLET LEG			
Pipe length	27	25	m
Pipe internal diameter	133.3	208.3	mm
Number of pipes per sector	2	3	–
OUTLET LEG			
Pipe length	3	6.1	m
Pipe internal diameter	160.3	208.3	mm
Number of pipes per sector	1	1	–
OUTLET LEG – IN PORT MANIFOLD			
Pipe length	17.5	9.7	m
Pipe internal diameter	160.3	258.8	mm
Number of pipes per sector	1	1	–

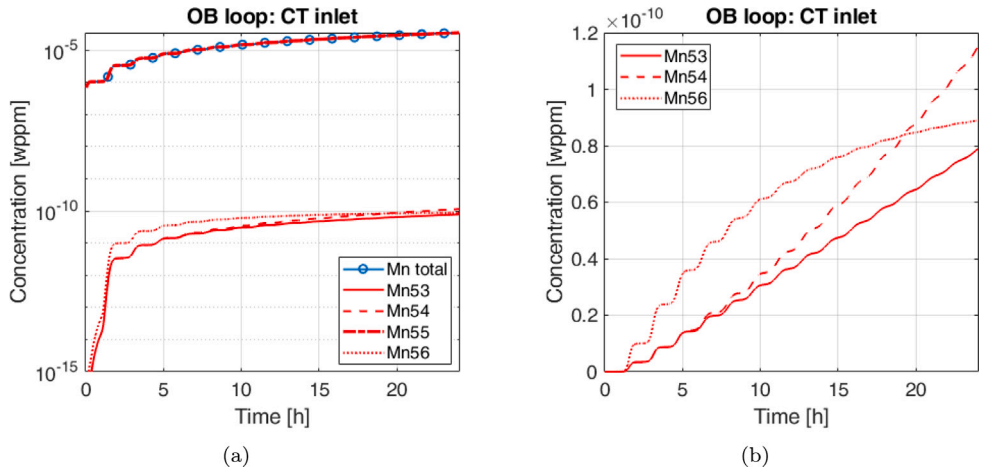

Fig. 5. Evolution of manganese concentration in the OB loop at the inlet of the system for the removal of ACPs; (a) logarithmic scale view of all Mn isotopes and total Mn concentration, and (b) expanded view of ^{53}Mn, ^{54}Mn and ^{56}Mn curves.

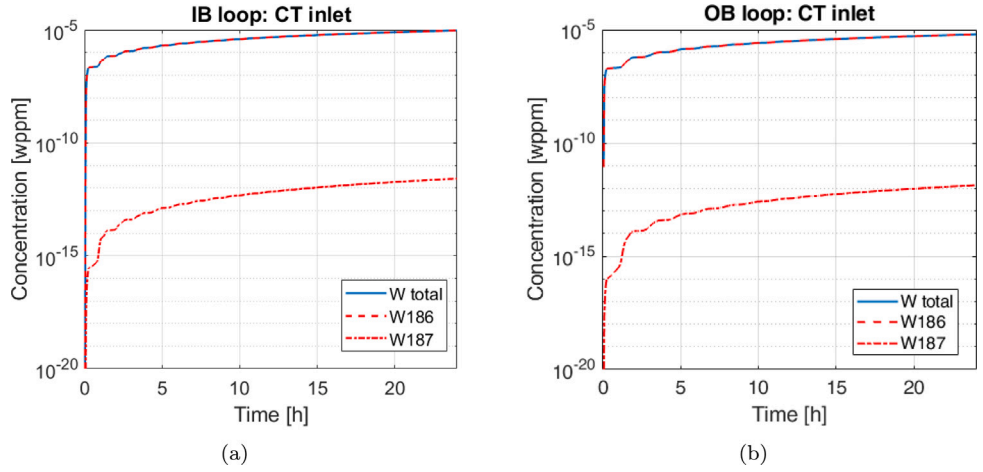

Fig. 6. Evolution of tungsten concentration at the inlet of the CT, for (a) IB circuit and (b) OB circuit.

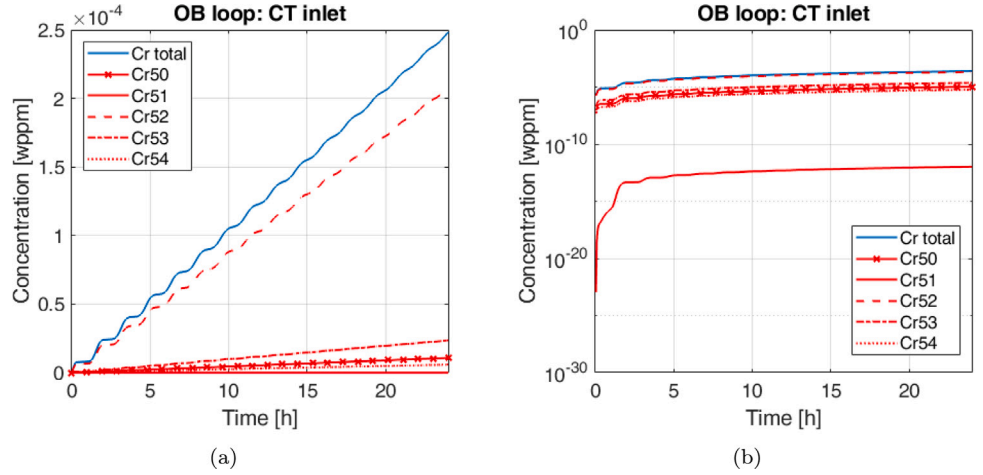

Fig. 7. Evolution of chromium concentration at the inlet of the system for the removal of ACPs (modelled here by the CT object, see Section 2) of the OB loop, (a) on linear scale and (b) on logarithmic scale, to show the buildup of ^{51}Cr .

expectations; however it must be noted that the results presented in this work may not necessarily reflect the real behaviour of the system, due to the assumption made for the development of the ACP transport and generation model (see Section 2) and for this test case (see Section 3.1), as well as to the uncertainties in the input parameters. Therefore, these results are only intended to illustrate the potential applications of the

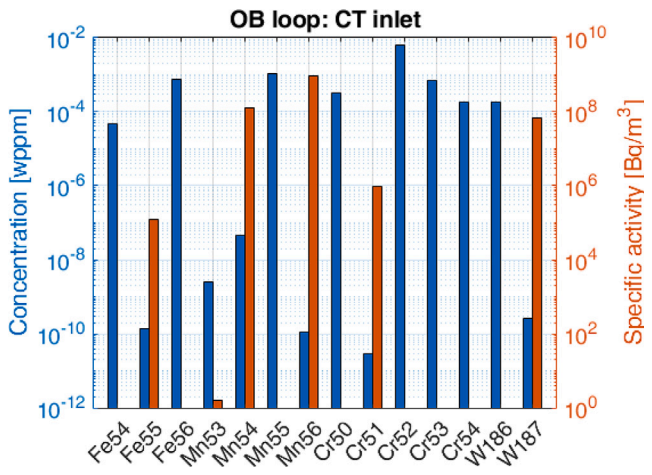

Fig. 8. Concentrations and specific activities of dispersed materials at the CT inlet in the OB loop after 30 days of transient, for the specific test case reported here.

model, rather than provide final estimates of the ACP concentrations in the WCLL PbLi loops.

4. Conclusions

The PbLi loop model implemented in the system-level GETTHEM code already included a preliminary modelling of the phenomena involved in the generation, transport, and removal of ACPs from the working fluid. However, the modelling of the ACP generation was limited to the assessment of the corrosion of solid particles from metal surfaces by means of the PbLi flow.

In this work, additional pieces of physics necessary for a comprehensive assessment of the ACP inventories are added to the PbLi loop model. Specifically, two source/sink terms have been added to the mass conservation equations for the corrosion products: one accounting for the activation of the corroded species carried within the working fluid, when exposed to the neutron flux inside the BB, and another for the radioactive decay of the species already activated. Moreover, providing as inputs the necessary nuclear data, such as cross sections for the activation reactions and decay constants, the model can be employed to simulate the generation and transport of an unlimited number of species within the PbLi.

To demonstrate the capability of the new ACP activation and decay models, a test case simulation has been performed for the WCLL IB and OB PbLi loops. A transient of 30 days of operation of the PbLi loops has been simulated, considering iron, chromium, manganese and tungsten, corroded from EUROFER97 and stainless steel structures, as dispersed materials carried by the working fluid. The main activation reactions undergone by these species in the BB are modelled. The evolution of iron, chromium, manganese and tungsten concentrations in PbLi during the simulated timespan have been shown, and the maximum activity due to the presence of active isotopes has been evaluated at the location within the different components of the WCLL PbLi loops where it reaches the maximum value, i.e. the cold trap inlet. The results show that the iron concentration reaches steady-state after $\sim$ 5 h in the OB and after $\sim$ 4 h in the IB, while chromium and manganese concentrations are well below their saturation concentrations at the end of the transient, so that they cannot be removed by the cold trap. On the other hand, the specific activity of the unstable isotopes of manganese and tungsten is non-negligible and should be further investigated in the future.

In perspective, the model for the ACP generation and transport shall be extended to include also the activation of structural materials in the BB and the chemical interaction between liquid metal and solid structure (for instance, to assess the redeposition of corroded species on solid surfaces, implementing specific correlations).

CRediT authorship contribution statement

Fabrizio Lisanti: Writing – review & editing, Writing – original draft, Software, Methodology, Formal analysis. **Alex Aimetta:** Writing – review & editing, Writing – original draft, Software, Methodology, Formal analysis. **Pietro Arena:** Project administration. **Roberto Bonifetto:** Writing – review & editing, Supervision, Methodology, Conceptualization. **Antonio Froio:** Writing – review & editing, Supervision, Methodology, Conceptualization.

Declaration of competing interest

The authors declare the following financial interests/personal relationships which may be considered as potential competing interests: Antonio Froio reports financial support was provided by Euratom Research and Training Programme. If there are other authors, they declare that they have no known competing financial interests or personal relationships that could have appeared to influence the work reported in this paper.

Acknowledgements

This work has been carried out within the framework of the EUROfusion Consortium, funded by the European Union via the Euratom Research and Training Programme (Grant Agreement No 101052200 — EUROfusion). Views and opinions expressed are however those of the author(s) only and do not necessarily reflect those of the European Union or the European Commission. Neither the European Union nor the European Commission can be held responsible for them.

Data availability

Data will be made available on request.

References

[1] P. Arena, A. Del Nevo, F. Moro, S. Noce, R. Mozzillo, V. Imbriani, F. Giannetti, F. Edemetti, A. Froio, L. Savoldi, S. Siriano, A. Tassone, F. Roca Urgorri, P.A. Di Maio, I. Catanzaro, G. Bongiovì, The DEMO Water-Cooled Lead–Lithium Breeding Blanket: Design Status at the End of the Pre-Conceptual Design Phase, Appl. Sci. 11 (24) (2021) http://dx.doi.org/10.3390/app112411592.

[2] A. Froio, C. Bachmann, F. Cismondi, L. Savoldi, R. Zanino, Dynamic thermal-hydraulic modelling of the EU DEMO HCPB breeding blanket cooling loops, Prog. Nucl. Energy 93 (2016) 116–132, http://dx.doi.org/10.1016/j.pnucene.2016.08.007.

[3] A. Froio, F. Casella, F. Cismondi, A. Del Nevo, L. Savoldi, R. Zanino, Dynamic thermal-hydraulic modelling of the EU DEMO WCLL breeding blanket cooling loops, Fusion Eng. Des. 124 (2017) 887–891, http://dx.doi.org/10.1016/j.fusengdes.2017.01.062, Proceedings of the 29th Symposium on Fusion Technology (SOFT-29) Prague, Czech Republic, September 5-9, 2016.

[4] A. Froio, A. Batti, A. Del Nevo, L. Savoldi, A. Spagnuolo, R. Zanino, Implementation of a system-level magnetohydrodynamic model in the GETTHEM code for the analysis of the EU DEMO WCLL Breeding Blanket, Proc. TOFE (2020).

[5] R. Bonifetto, N. Abrate, A. Froio, F. Lisanti, F. Papa, M. Utili, A. Venturini, Modelling the PbLi flow including tritium transport and permeation with GETTHEM, Nucl. Mater. Energy 37 (2023) 101500, http://dx.doi.org/10.1016/j.nme.2023.101500, URL https://www.sciencedirect.com/science/article/pii/S2352179123001394.

[6] F. Lisanti, P. Arena, R. Bonifetto, A. Froio, F.A.H. González, G.A. Spagnuolo, R. Zanino, Modeling the transport of activated corrosion products in the WCLL PbLi loop for ITER and the EU DEMO with the GETTHEM code, IEEE Access 11 (2023) 22614–22628, http://dx.doi.org/10.1109/ACCESS.2023.3252905.

[7] J. Sannier, M. Broc, T. Flament, A. Terlain, Corrosion of austenitic and martensitic stainless steels in flowing Pb17Li alloy, Fusion Eng. Des. 14 (3) (1991) 299–307, http://dx.doi.org/10.1016/0920-3796(91)90013-G.

[8] R. Franke, F. Casella, M. Sielemann, M. Proelss, M. Wetter, Standardization of Thermo-Fluid Modeling in Modelica.Fluid, in: Proceedings of the 7th Modelica Conference, 20-22 September 2009, 2009.
[9] J. Gorley, Initial MCNP6 Release Overview - MCNP6 Version 1.0., Tech. Rep. LA-UR-13-22934, 2013.
[10] A. Plompen, O. Cabellos, C. De Saint Jean, et al., The joint evaluated fission and fusion nuclear data library, JEFF-3.3, Eur. Phys. J. A 56 (2020) http://dx.doi.org/10.1140/epja/s10050-020-00141-9.
[11] D.A. Brown, M.B. Chadwick, R. Capote, A.C. Kahler, A. Trkov, M.W. Herman, A.A. Sonzogni, Y. Danon, A.D. Carlson, M. Dunn, D.L. Smith, G.M. Hale, G. Arbanas, R. Arcilla, C.R. Bates, B. Beck, B. Becker, F. Brown, R.J. Casperson, J. Conlin, D.E. Cullen, M.A. Descalle, R. Firestone, T. Gaines, K.H. Guber, A.I. Hawari, J. Holmes, T.D. Johnson, T. Kawano, B.C. Kiedrowski, A.J. Koning, S. Kopecky, L. Leal, J.P. Lestone, C. Lubitz, J.I. Márquez Damián, C.M. Mattoon, E.A. McCutchan, S. Mughabghab, P. Navratil, D. Neudecker, G.P.A. Nobre, G. Noguere, M. Paris, M.T. Pigni, A.J. Plompen, B. Pritychenko, V.G. Pronyaev, D. Roubtsov, D. Rochman, P. Romano, P. Schillebeeckx, S. Simakov, M. Sin, I. Sirakov, B. Sleaford, V. Sobes, E.S. Soukhovitskii, I. Stetcu, P. Talou, I. Thompson, S. van der Marck, L. Welser-Sherrill, D. Wiarda, M. White, J.L. Wormald, R.Q. Wright, M. Zerkle, G. Žerovnik, Y. Zhu, ENDF/B-VIII.0: the 8^{th} major release of the nuclear reaction data library with CIELO-project cross sections, new standards and thermal scattering data, Nucl. Data Sheets 148 (2018) 1–142.
[12] R. Macfarlane, D.W. Muir, R.M. Boicourt, A.C. Kahler III, J.L. Conlin, The NJOY Nuclear Data Processing System, Version 2016, Tech. Rep., Los Alamos National Laboratory (LANL), 2017, http://dx.doi.org/10.2172/1338791.
[13] Los Alamos National Laboratory, NJOY, 2016, https://github.com/njoy.
[14] P. Arena, A. Del Nevo, F. Moro, S. Noce, R. Mozzillo, V. Imbriani, F. Giannetti, F. Edemetti, A. Froio, L. Savoldi, S. Siriano, A. Tassone, F. Roca Urgorri, P.A. Di Maio, I. Catanzaro, G. Bongiovì, The DEMO Water-Cooled Lead–Lithium Breeding Blanket: Design Status at the End of the Pre-Conceptual Design Phase, Appl. Sci. 11 (24) (2021) http://dx.doi.org/10.3390/app112411592.
[15] R. Mozzillo, M. Utili, A. Venturini, A. Tincani, C. Gliss, Integration of LiPb loops for WCLL BB of European DEMO, Fusion Eng. Des. 167 (2021) 112379, http://dx.doi.org/10.1016/j.fusengdes.2021.112379.
[16] G. Stankunas, F. Moro, A. Tidikas, Activity and decay heat calculations for the European DEMO WCLL breeder blanket module including activated LiPb flow, Fusion Eng. Des. 146 (2019) 2552–2556, http://dx.doi.org/10.1016/j.fusengdes.2019.04.038.
[17] A. Aiello, LLE_ACP_TechNote, Tech. Rep., 2019, F4E_D_2HHTUC v2.2.
[18] F. Moro, S. Noce, Private comunication, 2024.
[19] E. Martelli, A. Del Nevo, P. Arena, G. Bongiovì, G. Caruso, P. Di Maio, M. Eboli, G. Mariano, R. Marinari, F. Moro, et al., Advancements in DEMO WCLL breeding blanket design and integration, Int. J. Energy Res. 42 (1) (2018) 27–52.
[20] E. Sartori, G. Panini, ZZ groupstructures, vitamin-J, xmas, ECCO-33, ECCO2000 standard goup structures, 1991.
[21] A. Venturini, F. Papa, C. Alberghi, D. Martelli, R. Bonifetto, A. Froio, F. Lisanti, B. Garcinuño, F.R. Urgorri, I. Fernández-Berceruelo, et al., Progresses in the development of the tritium extraction and removal system for the water-cooled lithium-lead breeding blanket in EUROfusion, Fusion Eng. Des. 216 (2025).